

DiffPF: Differentiable Particle Filtering with Generative Sampling via Conditional Diffusion Models

Ziyu Wan and Lin Zhao

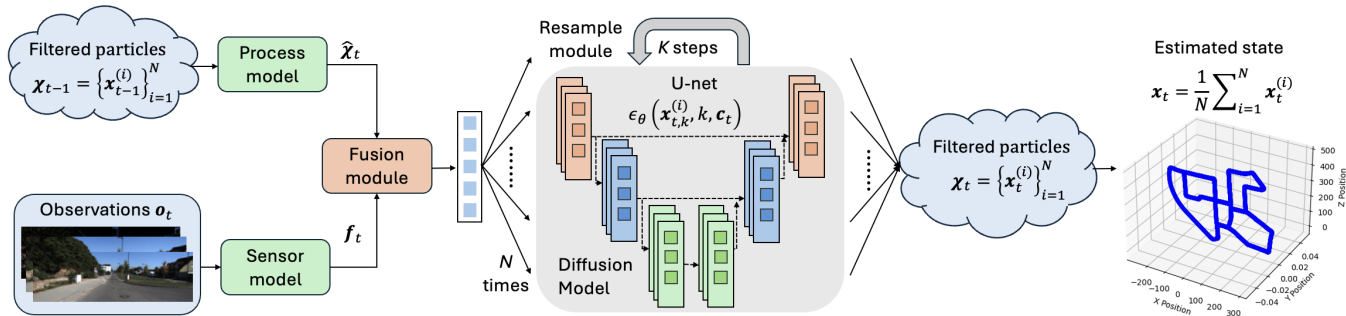


Fig. 1: An illustration of DiffPF applied to the KITTI visual odometry dataset. DiffPF is a differentiable particle filter that employs a conditional diffusion model as an implicit posterior sampler. Conditioned on the predicted particles and the current observation, the diffusion model performs iterative denoising to sample equally-weighted particles that approximate the posterior distribution. This approach enables accurate state estimation in high-dimensional and multimodal scenarios, outperforming existing differentiable filters.

Abstract—This paper proposes DiffPF, a differentiable particle filter that leverages diffusion models for state estimation in dynamic systems. Unlike conventional differentiable particle filters—which require importance weighting and typically rely on predefined or low-capacity proposal distributions. DiffPF learns a flexible posterior sampler by conditioning a diffusion model on predicted particles and the current observation. This enables accurate, equally-weighted sampling from complex, high-dimensional, and multimodal filtering distributions. We evaluate DiffPF across a range of scenarios, including both unimodal and highly multimodal distributions, and test it on simulated as well as real-world tasks, where it consistently outperforms existing filtering baselines. In particular, DiffPF achieves an 82.8% improvement in estimation accuracy on a highly multimodal global localization benchmark, and a 26% improvement on the real-world KITTI visual odometry benchmark, compared to state-of-the-art differentiable filters. To the best of our knowledge, DiffPF is the first method to integrate conditional diffusion models into particle filtering, enabling high-quality posterior sampling that produces more informative particles and significantly improves state estimation. The code will be made available online upon acceptance.

I. INTRODUCTION

Estimating the hidden state of a dynamic system from partial and noisy observations is a core challenge across a wide range of applications, including navigation [1], control [2], and robotics [3]. Kalman filters and their extensions [4] have long served as standard tools within the Bayesian filtering framework. However, their reliance on linearity and Gaussian noise assumptions severely limits their applicability to real-world systems that are often nonlinear, high-dimensional and exhibit multimodal behaviors.

These authors are with the Department of Electrical and Computer Engineering, National University of Singapore, 4 Engineering Drive 3, 117583 Singapore, Singapore wzyu@u.nus.edu, elezhli@nus.edu.sg

An alternative line of work, particle filters, avoids these restrictive assumptions by representing the posterior distribution with a set of weighted samples instead of relying on closed-form expressions. Bootstrap particle filter [5], one of the most commonly used algorithms, draws particles from the transition model and assigns weights based on observation likelihoods. Rao-Blackwellized particle filter [6] further improves efficiency by analytically marginalizing part of the latent state using parametric inference, thereby reducing sampling variance. However, these methods still rely on manually designed or limited-capacity proposals and are prone to sample degeneracy, particularly in high-dimensional or perceptually complex domains.

Recent developments in deep learning have introduced data-driven alternatives to traditional state estimation methods. Deep state-space models (DSSMs) [7] provide a unified framework capable of capturing nonlinear latent dynamics and processing high-dimensional inputs, making them particularly suited for complex real-world environments. Differentiable Particle Filters (DPFs), a class of methods that embed sample-based filtering into DSSMs [8], [9], enable end-to-end learning of recursive Bayesian inference over learned dynamics and observation models. However, most DPFs still inherit several limitations from classical particle filtering. The proposal distributions used in DPFs are often either hand-crafted or limited in capacity, making it difficult to match the true filtering posterior [10]. Furthermore, they rely on importance sampling, which necessitates explicit weighting of particles—a process that becomes increasingly unreliable in high-dimensional or highly multimodal settings due to particle degeneracy.

To overcome these challenges, we employ diffusion models as powerful implicit samplers, capable of capturing rich and multimodal posterior distributions. This allows for

a more expressive and learnable formulation of the state update step within the filtering process. Specifically, DiffPF employs a diffusion model for state update, conditioned on both the predicted particles and the current observation to generate refined posterior samples. An example application of DiffPF on the KITTI visual odometry benchmark [11] is shown in Figure 1. DiffPF departs from particle filtering by eliminating the reliance on importance sampling and explicit proposal distributions. Instead, it leverages a diffusion model to sample directly from the filtering posterior, enabling accurate inference without the need for particle weighting. This sampling-based yet weight-free approach naturally avoids particle degeneracy and, consequently, eliminates the need for the non-differentiable resampling step, while supporting multimodal and high-dimensional distributions.

The main contributions of this paper are summarized as follows:

- We introduce a differentiable filtering framework that employs diffusion models for latent states estimation. To the best of our knowledge, this is the first application of diffusion models in differentiable particle filtering.
- Our method enables high-quality, weight-free inference by implicitly modeling and sampling from the posterior distribution. This eliminates particle degeneracy and removes the need for manually designed proposals, while supporting high-dimensional, multimodal posteriors in a fully differentiable and end-to-end trainable paradigm.
- We evaluate DiffPF across a range of synthetic and real-world scenarios, covering both unimodal and multimodal distributions. Across these benchmarks, our approach achieves significant improvements over existing state-of-the-art differentiable filtering methods.

II. RELATED WORK

A. Particle filter

Particle filters (PFs) are a class of sequential Monte Carlo (SMC) methods widely used for recursive state estimation in nonlinear and non-Gaussian systems [12]. Classical particle filters, such as the Bootstrap Filter [5], are built on the Sampling-Importance-Resampling (SIR) framework [13], which approximates the filtering distribution using weighted particles. While theoretically general, these methods often struggle in practice due to particle degeneracy—where most weights collapse to near zero—and the difficulty of designing effective proposal distributions, especially in high-dimensional or perceptually complex environments.

Several extensions have been proposed to improve the sampling efficiency of particle filters. General importance sampling filters [14] aim to use more informed proposal distributions that better align with the true posterior, while the Auxiliary Particle Filter (APF) [15] incorporates observation information to guide the selection of particles before propagation. In parallel, sequential MCMC methods [16] replace the standard sampling step in particle filters with Markov chain updates over full or partial trajectories, allowing for posterior-consistent sampling. Particle MCMC

(PMCMC) [17] integrates particle filtering into Markov chain Monte Carlo algorithms for joint parameter and state inference. Detailed treatments of these and other developments in particle filtering can be found in [13].

B. Differentiable Particle Filters

The aforementioned methods often assume known system dynamics or observation models, which often do not hold in real-world scenarios [18]. Differentiable particle filters [8]–[10], [19]–[23] address this by integrating neural networks into the filtering process, enabling end-to-end learning from data.

Most DPFs model transition dynamics by mapping previous states to the next latent state using either fully connected networks [9], [10], recurrent architectures such as LSTMs and GRUs [20], [23], or fixed parametric forms with learnable noise parameters [22]. Observation models are typically implemented as neural networks that either output the parameters of a predefined distribution (e.g., the mean and variance of a Gaussian) [23] or produce unnormalized scores interpreted as pseudo-likelihoods [19]. While effective in simple scenarios, these designs are often restricted to specific distribution families and struggle to represent complex or multimodal posteriors, limiting the expressiveness of the resulting filtering distributions and motivating the need for a more flexible and general framework.

The proposal distribution, which guides particle sampling, is typically handcrafted [24], [25] or implemented as a neural network conditioned on the current observation and possibly past states. In many DPFs, the transition model is reused as the proposal, and particles are often generated deterministically via regression rather than sampling, which leads to particle degeneracy [26], reduces particle quality, and constrains the representational capacity of the filtering distribution. Although [18] proposes using normalizing flows to sample from the proposal distribution, the method remains confined to the importance sampling framework and suffers from accumulated estimation errors due to sampling from multiple distributions simultaneously. To enable gradient-based learning, DPFs must address the non-differentiability of traditional resampling operations. Several methods replace hard resampling with differentiable approximations [27], such as soft-resampling [10] and entropy-regularized optimal transport solvers [19]. While these approximations allow gradients to flow through resampling steps, they often introduce additional computational complexity or require task-specific tuning, and particle degeneracy can still persist.

C. Diffusion Models for Probabilistic Modeling

Recent advances in generative modeling have highlighted diffusion models as effective tools for capturing intricate, multimodal distributions across a range of data types. These models operate by progressively denoising latent variables [28], [29], making them particularly adept at representing uncertainty and complex data structures.

In the domain of robotics, such approaches as Diffusion Policy [30] and NoMaD [31] have demonstrated the effec-

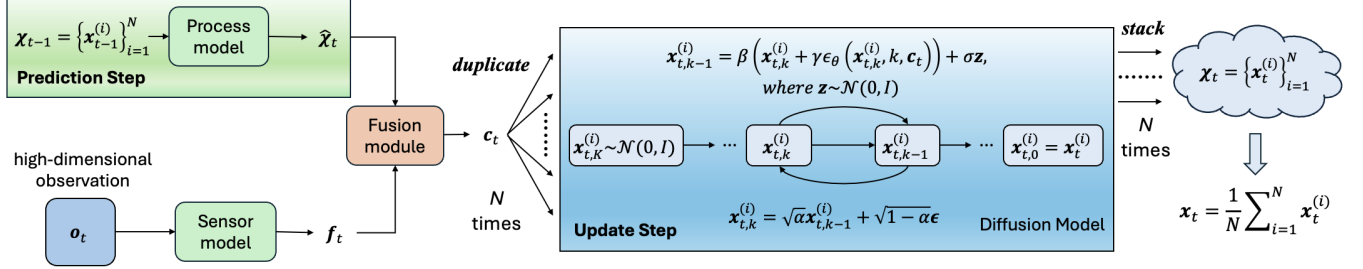


Fig. 2: At time t , the estimated particles from time $t-1$ are propagated through the process model to obtain a prior distribution over the current state. Simultaneously, the observation \mathbf{o}_t is encoded into a feature representation. These two sources of information are jointly used as the condition for a conditional diffusion model, which iteratively refines a set of noisy latent samples to generate equally-weighted particles that approximate the filtering posterior.

tiveness of conditional diffusion models in generating action sequences by capturing the inherently multi-modal nature of action distributions [32]. Meanwhile, diffusion models have gained significant attention for their effectiveness in trajectory generation [33], [34]. Building on the success of these tasks, we explore their potential in state estimation. Existing attempts include introducing diffusion models into Kalman filters [35]. We further develop a novel sample-based framework that integrates diffusion models into differentiable particle filtering, and propose end-to-end efficient training algorithms to facilitate the filter design. To our knowledge, this is the first such integration, and it significantly improves estimation accuracy across a variety of scenarios.

III. METHOD

In sequential inference, a Bayesian filter aims to recursively estimate the current state \mathbf{x}_t via the posterior distribution $\text{post}(\mathbf{x}_t) := p(\mathbf{x}_t \mid \mathbf{o}_{1:t}, \mathbf{a}_{1:t})$, conditioned on all observations and actions up to time t . Under the Markov assumption, all relevant information from past observations $\mathbf{o}_{1:t}$ and actions $\mathbf{a}_{1:t}$ is captured by the current posterior $\text{post}(\mathbf{x}_t)$. By exploiting the conditional independence of observations and actions given the latent state, the inference proceeds recursively in two steps [9], [36]. In the prediction step, the posterior from the previous timestep is propagated through the system’s transition dynamics to yield a prior over the current state:

$$p(\mathbf{x}_t \mid \mathbf{o}_{1:t-1}, \mathbf{a}_{1:t}) = \int p(\mathbf{x}_t \mid \mathbf{x}_{t-1}, \mathbf{a}_t) \text{post}(\mathbf{x}_{t-1}) d\mathbf{x}_{t-1}. \quad (1)$$

This predicted prior $p(\mathbf{x}_t \mid \mathbf{o}_{1:t-1}, \mathbf{a}_{1:t})$ implicitly reflects all relevant past information, as conveyed by the previous posterior and the process model. In the update step, the filter updates its estimate of the current state by integrating the prior distribution, obtained from the prediction step, with the latest observation \mathbf{o}_t . As illustrated in Figure 2, our method follows this two-step Bayesian filtering procedure and represents the posterior $\text{post}(\mathbf{x}_t)$ using a set of equally weighted particles $\chi_t := \{\mathbf{x}_t^{(i)}\}_{i=1}^N$. The remainder of this section details each component of the proposed framework.

A. System and Perception Modeling

Given a set of N particles $\{\mathbf{x}_{t-1}^{(i)}\}_{i=1}^N$ representing the posterior at time $t-1$, we apply a process model to obtain predicted particles $\hat{\chi}_t := \{\hat{\mathbf{x}}_t^{(i)}\}_{i=1}^N$ for the current step. Specifically, each particle is propagated through a learnable or given process model f_{dyn} as:

$$\hat{\mathbf{x}}_t^{(i)} = f_{\text{dyn}}(\mathbf{x}_{t-1}^{(i)}, \mathbf{a}_t), \quad (2)$$

where \mathbf{a}_t is the action at time t . Through this step, the relevant information from the action sequence $\mathbf{a}_{1:t}$ and past observations $\mathbf{o}_{1:t-1}$ is encoded into the predicted particle set $\{\hat{\mathbf{x}}_t^{(i)}\}_{i=1}^N$. The process model f_{dyn} can be defined using either parametric forms based on system knowledge, or learned from data using neural networks such as Multi-Layer Perceptrons (MLPs), stochastic models [37], or generative approaches like normalizing flows [38].

In parallel, the current observation \mathbf{o}_t is processed by a neural sensor model g_{obs} to extract observation features:

$$\mathbf{f}_t = g_{\text{obs}}(\mathbf{o}_t). \quad (3)$$

This feature representation encodes perceptual information relevant to the latent state.

Unlike conventional differentiable filters that rely on predefined distribution families or manually specified noise models to represent the dynamics and observation processes, our approach imposes fewer assumptions and offers better generalization across scenarios.

To combine the information from the prior and observation \mathbf{o}_t , we incorporate a learnable fusion mechanism that aggregates the predicted particles and perceptual embeddings:

$$\mathbf{c}_t = \text{Fusion}(\mathbf{f}_t, \{\hat{\mathbf{x}}_t^{(i)}\}_{i=1}^N), \quad (4)$$

where \mathbf{c}_t aggregates temporal information from $\mathbf{o}_{1:t}$ and $\mathbf{a}_{1:t}$ via the process and sensor models, and serves as the conditioning input for the subsequent diffusion process.

B. Update Step

Update step refines the prior belief over the current state by incorporating the latest observation. In conventional DPFs, the update is typically implemented by assigning importance weights to particles based on an observation model, followed by resampling to mitigate particle degeneracy. However,

these procedures often require carefully designed likelihood functions and involve non-differentiable operations. In contrast, our method performs the update implicitly through a conditional diffusion model. Specifically, we make an assumption that

$$\text{post}(\mathbf{x}_t) \approx p(\mathbf{x}_t | \mathbf{c}_t). \quad (5)$$

This assumption is justified because \mathbf{c}_t captures all temporal information from $\mathbf{o}_{1:t}$ and $\mathbf{a}_{1:t}$. Instead of sampling directly from the intractable posterior distribution $p(\mathbf{x}_t | \mathbf{o}_{1:t}, \mathbf{a}_{1:t})$, we choose to sample from the approximated distribution $p(\mathbf{x}_t | \mathbf{c}_t)$. This yields a set of particles $\{\mathbf{x}_t^{(i)}\}_{i=1}^N$, from which we can derive:

$$\begin{aligned} \text{post}(\mathbf{x}_t) &= \eta \sum_{i=1}^N \frac{p(\mathbf{x}_t^{(i)} | \mathbf{o}_{1:t}, \mathbf{a}_{1:t})}{p(\mathbf{x}_t^{(i)} | \mathbf{c}_t)} \delta(\mathbf{x}_t - \mathbf{x}_t^{(i)}), \\ &\approx \eta \sum_{i=1}^N \delta(\mathbf{x}_t - \mathbf{x}_t^{(i)}) = \frac{1}{N} \sum_{i=1}^N \delta(\mathbf{x}_t - \mathbf{x}_t^{(i)}), \end{aligned} \quad (6)$$

where $\delta(\cdot)$ denotes the Dirac function and η is a normalization constant. This indicates that all sampled particles share equal weights, thereby eliminating the need for weighting or resampling.

Diffusion models have been shown to approximate arbitrarily complex probability distributions by learning time-dependent score functions that guide the reversal of a noise-perturbed process [39]. In our case, a conditional diffusion model is trained to approximate $p(\mathbf{x}_t | \mathbf{c}_t)$ and generate particle samples. Specifically, we instantiate a reverse diffusion process with a Denoising Diffusion Probabilistic Model (DDPM), which iteratively refines a random Gaussian sample toward the target posterior distribution. We begin by drawing an initial Gaussian sample:

$$\mathbf{x}_{t,K}^{(i)} \sim \mathcal{N}(0, I), \quad (7)$$

where K is the total number of reverse diffusion steps. At each step k , the model predicts the noise component $\epsilon_\theta(\mathbf{x}_{t,k}^{(i)}, k, \mathbf{c}_t)$, which subsequently serves to infer a cleaner approximation of the sample at timestep $k-1$:

$$\begin{aligned} \mathbf{x}_{t,k-1}^{(i)} &= \frac{1}{\sqrt{\alpha}} \left(\mathbf{x}_{t,k}^{(i)} - \frac{1-\alpha}{\sqrt{1-\bar{\alpha}}} \epsilon_\theta(\mathbf{x}_{t,k}^{(i)}, k, \mathbf{c}_t) \right) + \sigma \mathbf{z}, \\ &:= \beta(\mathbf{x}_{t,k}^{(i)} + \gamma \epsilon_\theta(\mathbf{x}_{t,k}^{(i)}, k, \mathbf{c}_t)) + \sigma \mathbf{z}. \end{aligned} \quad (8)$$

Here $\mathbf{z} \sim \mathcal{N}(0, I)$, and $\mathbf{x}_{t,k}^{(i)}$ refers to the i -th corrupted sample at diffusion step k . α , $\bar{\alpha}$, σ are fixed noise schedule parameters as defined in [40], while β and γ are scaling terms introduced for simplicity. This stochastic refinement continues recursively until $k=0$, yielding the final particle sample

$$\mathbf{x}_{t,0}^{(i)} = \mathbf{x}_t^{(i)}. \quad (9)$$

This reverse diffusion process is repeated N times to produce the final particle set $\mathcal{X}_t = \{\mathbf{x}_t^{(i)}\}_{i=1}^N$. As all particles are equally weighted, the final estimate is given by the average over the particle set

$$\mathbf{x}_t = \frac{1}{N} \sum_{i=1}^N \mathbf{x}_t^{(i)} \quad (10)$$

By leveraging a diffusion model for the update step, our framework effectively approximates complex and multimodal posterior distributions and samples high-quality samples while preserving full differentiability. Moreover, it removes the need for handcrafted proposals and circumvents the weighting and resampling procedures required in importance sampling frameworks, thereby mitigating inefficiencies and avoiding particle degeneracy.

C. End-to-End Training

Training the denoising diffusion model involves maintaining a forward diffusion process and learning to reverse this process. Instead of explicitly iterating through each diffusion step, we utilize a closed-form solution to efficiently sample a noisy version of the ground truth state $\mathbf{x}_{t,0}^*$ at an arbitrary diffusion timestep k :

$$\mathbf{x}_{t,k}^* = \sqrt{\alpha} \mathbf{x}_{t,0}^* + \sqrt{1-\bar{\alpha}} \epsilon, \quad \epsilon \sim \mathcal{N}(0, I), \quad (11)$$

where ϵ denotes a Gaussian noise. The model is then trained to denoise $\mathbf{x}_{t,k}^*$ by predicting the added noise ϵ , conditioned on the timestep k and the fusion vector \mathbf{c}_t . A U-Net ϵ_θ (see Figure 1) is used for this task, and training minimizes the mean squared error between predicted and actual noise:

$$\mathcal{L} = \mathbb{E}_{\mathbf{x}_{t,k}^*, k, \mathbf{c}_t, \epsilon} \left[\left\| \epsilon - \epsilon_\theta(\mathbf{x}_{t,k}^*, k, \mathbf{c}_t) \right\|^2 \right]. \quad (12)$$

Each training iteration consists of the following procedure:

- (1) Draw a ground truth state $\mathbf{x}_{t,0}^*$ from the data;
- (2) Sample a timestep k and generate its noisy version $\mathbf{x}_{t,k}^*$ using (11);
- (3) Use ϵ_θ to predict the noise from $\mathbf{x}_{t,k}^*$, k , and \mathbf{c}_t ;
- (4) Update model parameters via minimizing the loss (12).

Importantly, all components of the system—including the process model, observation model, and fusion module—are trained end-to-end along with the diffusion model to ensure consistency in optimization.

IV. EXPERIMENTS

We evaluate DiffPF across three challenging state estimation tasks: (1) a synthetic image-based object tracking task, as introduced in [22], [41]; (2) a simulated global localization task with pronounced multimodality, based on [9], [19]; and (3) the real-world KITTI visual odometry benchmark [11].

We compare DiffPF against a comprehensive set of baselines in the following experiments, including the Deep State-Space Model (Deep SSM) [7], Particle Filter Recurrent Neural Networks (PFRNNs) [23], Particle Filter Networks (PFNets) [10], Normalizing Flow-based Differentiable Particle Filters (NF-DPFs) [18], Autoencoder Sequential Monte Carlo (AESMC) and its bootstrap variant (AESMC-Bootstrap) [24], [25], as well as other differentiable filtering and smoothing methods [22], [42]. Our methods were trained and evaluated on a workstation equipped with an NVIDIA GeForce RTX 4080 GPU and an Intel i7-14700KF CPU.

Experimental results demonstrate that DiffPF generalizes well across all test scenarios, achieves significantly higher state estimation accuracy compared to existing differentiable filters, and maintains practical inference efficiency.

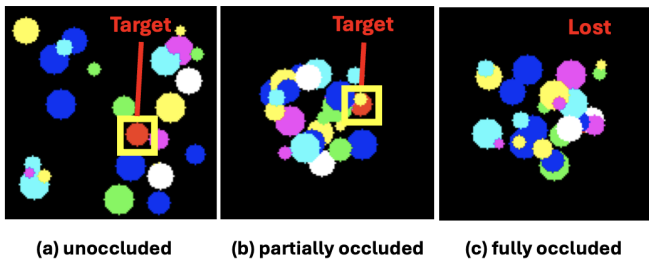


Fig. 3: A sequence of three frames with the target disk indicated by a yellow box. The frames illustrate three different levels of occlusion caused by interfering disks.

A. Vision-based Disk Tracking

Overview: The objective is to estimate the motion path of a specific disk within a crowded two-dimensional environment where numerous distractor disks move simultaneously. The position of the target disk is treated as the latent state. The main challenge of this task lies in the varying degrees of occlusion that occur during the target’s movement, as shown in Fig.3, which introduces dynamic uncertainty into the observations. For filtering methods, it is essential to effectively leverage both the temporal information derived from prediction and the information extracted from the current observations.

Data: We divide the dataset into 500 sequences for training and 50 for testing, with each sequence consisting of 50 RGB images at a resolution of 128×128 pixels following [22]. Each image contains a target disk and 25 distractor disks. The target disk consistently appears in red with a fixed radius of 7 pixels while the remaining 25 distractor disks vary in both size and color, with radii randomly selected from 3 to 10 pixels, and colors sampled from a predefined palette same as [18]. All disks are initially placed uniformly across the frame. The dynamics of all disks follow

$$\begin{cases} \mathbf{x}_{t+1}^* = \mathbf{x}_t^* + \mathbf{v}_t^* + \boldsymbol{\omega}_{x,t} \\ \mathbf{v}_{t+1}^* = \mathbf{v}_t^* - f_p \mathbf{x}_t^* - f_d \|\mathbf{v}_t^*\|^2 \text{sgn}(\mathbf{v}_t^*) + \boldsymbol{\omega}_{v,t}, \end{cases} \quad (13)$$

where \mathbf{x}_t^* and \mathbf{v}_t^* denote the position and velocity at time t ; $f_p = 0.05$ is a coefficient that pulls the object toward the origin; $f_d = 0.0075$ controls the strength of velocity damping; $\boldsymbol{\omega}_{x,t}$ and $\boldsymbol{\omega}_{v,t}$ are Gaussian noise; and $\text{sgn}(\cdot)$ returns the sign of a vector component-wise.

Implementation: The number of particles is set to 10. At time step t , we use the given velocity \mathbf{v}_t^* as input to generate a prior estimate of $\mathbf{x}_{t-1}^{(i)}$. The following formulation serves as our process model:

$$\hat{\mathbf{x}}_t^{(i)} = \mathbf{x}_{t-1}^{(i)} + \mathbf{v}^* \quad (14)$$

Due to the imperfection of the process model, observation \mathbf{o}_t is used to correct the prior estimate. We adopt the network architecture from [18] as our sensor model. To integrate $\{\hat{\mathbf{x}}_t^{(i)}\}_{i=1}^N$ with \mathbf{o}_t , we first convert the $\{\hat{\mathbf{x}}_t^{(i)}\}_{i=1}^N$ into a heatmap. The observation \mathbf{o}_t is encoded by the sensor model, while the heatmap is processed by a separate network with the same architecture. The outputs of both networks are then concatenated to form the feature representation \mathbf{c}_t , which

are used as conditions for the diffusion model. The noise estimator in the diffusion model is implemented as a 3-layer U-Net.

Results: We evaluate our proposed DiffPF across three dimensions:

- 1) **Benchmarking.** We compare the DiffPF with several baselines, including DeepSSM, AESMC-Bootstrap, AESMC, PFRNN, PFNet, and NF-DPF, all of which adopt the same process and observation models where applicable.
- 2) **Ablation analysis.** We further investigate the design of our method through controlled experiments, including:
 - *Number of diffusion steps.* We compare two variants, **DiffPF(5s)** and **DiffPF(10s)**, which use 5 and 10 diffusion steps respectively;
 - *Introduction of the model prior.* We also evaluate **DiffPF(no pred)**, a variant with 10 diffusion steps that does not use the process model and relies only on observations.
- 3) **Inference efficiency.** We assess the runtime of the DiffPF under different diffusion step settings.

All methods are evaluated using the mean squared error (MSE) between the predicted and ground-truth trajectories of the target object. Results are summarized in Table I and Table II.

TABLE I: Experimental results for ablation analysis and baseline comparisons. Mean and standard deviation are computed from 5 independent runs with varying random seeds.

Setting	Model	MSE (pixels)
Prior Works	Deep SSM	5.91 ± 1.20
	AESMC Bootstrap	6.35 ± 1.15
	AESMC	5.85 ± 1.34
	PFRNN	6.12 ± 1.23
	PFNet	5.34 ± 1.27
	NF-DPF	3.62 ± 0.98
Diffusion Step	DiffPF (5s)	1.50 ± 0.02
	DiffPF (10s)	1.37 ± 0.03
Predicted State	DiffPF (no pred)	5.23 ± 0.18

TABLE II: Runtime performance for different numbers of diffusion steps. Mean and standard deviation are computed from 5 independent runs with varying random seeds.

Diffusion Step	K = 5	K = 10
Inference Frequency (Hz)	59.0 ± 2.75	39.2 ± 1.11

Comparison: As shown in Table II and Table I, we observe that:

1. DiffPF outperforms existing differentiable particle filters in both accuracy and consistency while requiring far fewer particles. Compared to NF-DPF, which also leverages generative modeling, it shows a 62.2 % improvement. Moreover, the significantly lower variance across runs highlights its robustness and reliability.

2. Using more diffusion steps improves estimation accuracy, suggesting that a longer denoising process enhances the model’s predictive capability. Moreover, incorporating the

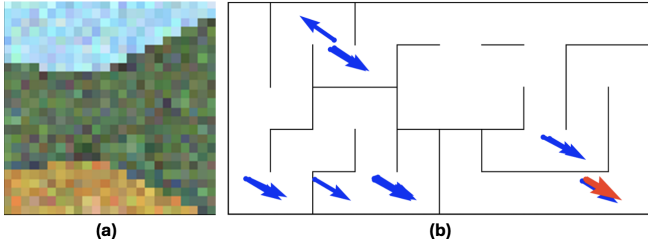


Fig. 4: (a) An example observation captured by the robot. (b) The red arrow indicates the true pose, while the blue arrows mark alternative poses in the map that yield similar observations, illustrating the multimodal nature of the observation-to-state mapping.

predicted state from the process model results in a 73.8% reduction in MSE, underscoring its substantial contribution to the overall performance.

3. Inference speed decreases with more diffusion steps. However, both settings sustain relatively high inference rates, demonstrating the practical applicability of DiffPF.

B. Global Localization

Overview: The task is to estimate the robot’s pose based on observed images and odometry data, within three maze environments simulated in DeepMind Lab [43]. The main challenge of this task lies in the highly multimodal nature of the observations: since we adopt the same experimental setup as in [9], unique textures have been deliberately removed from the environment, causing many locations in the maze to produce nearly identical images. An example of the observation image is shown in Fig 5, along with the corresponding candidate poses on the map.

Data: Consistent with [18], the dataset is divided into 900 training sequences and 100 test sequences, with each sequence containing 100 time steps. The ground truth state is defined as the robot’s position and orientation, denoted as $\mathbf{x}_t^* := (p_{t,x}^*, p_{t,y}^*, \theta_t^*)$, and the action \mathbf{a}_t^* is computed from the state difference between consecutive time steps, $\Delta \mathbf{x}_t^* = \mathbf{x}_t^* - \mathbf{x}_{t-1}^* = (\Delta p_{t,x}^*, \Delta p_{t,y}^*, \Delta \theta_t^*)$ as

$$\begin{aligned} u_t^* &= \cos(\theta_{t-1}^*) \cdot \Delta p_{t,x}^* + \sin(\theta_{t-1}^*) \cdot \Delta p_{t,y}^*, \\ v_t^* &= -\sin(\theta_{t-1}^*) \cdot \Delta p_{t,x}^* + \cos(\theta_{t-1}^*) \cdot \Delta p_{t,y}^*, \\ \mathbf{a}_t^* &:= (u_t^*, v_t^*, \Delta \theta_t^*), \end{aligned} \quad (15)$$

which corresponds to the robot’s velocity in its local frame. The original 32×32 RGB observations are randomly cropped to 24×24 and augmented with Gaussian noise ($\sigma = 20$) to introduce visual uncertainty.

Implementation: To effectively capture the uncertainty arising from the task’s multimodal structure, we use 20 particles in our filter. At time step t , we use the given input \mathbf{a}_t^* to generate a prior estimate of $\mathbf{x}_t^{(i)} = (p_{t,x}^{(i)}, p_{t,y}^{(i)}, \theta_t^{(i)})$. We form the process model as:

$$\hat{\mathbf{x}}_t^{(i)} = \begin{bmatrix} p_{t,x}^{(i)} + u_t^* \cos(\theta_t^{(i)}) + v_t^* \sin(\theta_t^{(i)}) \\ p_{t,y}^{(i)} + u_t^* \sin(\theta_t^{(i)}) - v_t^* \cos(\theta_t^{(i)}) \\ \theta_t + \Delta \theta_t^* \end{bmatrix} + \boldsymbol{\omega}_t, \quad (16)$$

where $\boldsymbol{\omega}_t$ denotes zero-mean Gaussian noise with covariance $\Sigma = \text{diag}(10^2, 10^2, 0.1^2)$. We adopt the same encoder

from [18] as our sensor model. To integrate $\{\hat{\mathbf{x}}_t^{(i)}\}_{i=1}^N$ with \mathbf{o}_t , We encode the observation \mathbf{o}_t using the sensor model and flatten the particle set $\{\hat{\mathbf{x}}_t^{(i)}\}_{i=1}^N$ into a vector. The two are concatenated to form the conditional input \mathbf{c}_t for the diffusion model. The noise estimator in the diffusion model is implemented as a 3-layer U-Net. The model is first pretrained using only observations, and then finetuned in a second training phase with particle-based priors integrated.

Results: DiffPF is compared with the same set of baselines as in the previous benchmark under a shared setup to assess overall performance. To analyze the contribution of the process model prior, we include a variant trained without it denoted as DiffPF (no pred). With the diffusion step set to 10, the model achieves an inference frequency of 45.5 Hz. All methods are evaluated using the root mean squared error (RMSE) between the predicted and ground-truth positions of the robot at the last step. The results are summarized in Table III.

TABLE III: RMSE between the predicted and ground-truth positions of the robot at the last step $t = 100$. Mean and standard deviation are computed from 5 independent runs with varying random seeds.

Method	Maze 1	Maze 2	Maze 3
Deep SSM	61.0 \pm 10.8	114.0 \pm 8.8	203.0 \pm 10.1
AESMC Bootstrap	56.5 \pm 11.5	115.6 \pm 6.8	220.6 \pm 11.1
AESMC	52.1 \pm 7.5	109.2 \pm 11.7	201.3 \pm 14.7
PFNet	51.4 \pm 8.7	120.3 \pm 8.7	212.1 \pm 15.3
PFRNN	54.1 \pm 8.9	125.1 \pm 8.2	210.5 \pm 10.8
NF-DPF	46.1 \pm 6.9	103.2 \pm 10.8	182.2 \pm 19.9
DiffPF (no pred)	137.0 \pm 3.8	213.0 \pm 5.8	414.6 \pm 12.3
DiffPF	12.3 \pm 0.3	11.2 \pm 0.3	25.7 \pm 2.7

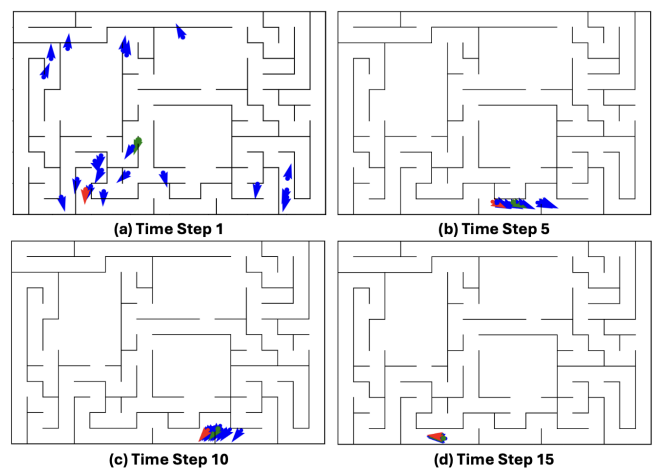


Fig. 5: Estimated poses at selected time steps from a sequence using DiffPF. Red arrows indicate the ground truth, green arrow represent the estimated pose, and blue arrows represent the particle set.

Comparison: As shown in Table III, DiffPF achieves superior performance over existing differentiable particle filters in terms of both accuracy and consistency, while operating with substantially fewer particles. Compared to NF-DPF—which also employs generative modeling—DiffPF

achieves improvements of 73.3%, 89.1%, and 85.9% in Maze 1, Maze 2, and Maze 3, respectively. Furthermore, the notably lower variance observed across multiple runs underscores its robustness and reliability. As shown in Fig. 5, even in the most complex and highly multimodal Maze 3 environment, DiffPF is able to rapidly converge to a pose close to the ground truth during the early stages, while other methods may require 50 or more steps to achieve similar accuracy, highlighting the strong representational and sampling capabilities of the diffusion model. Incorporating the process model prior yields RMSE reductions of 91.0%, 94.7%, and 93.8% in the three maze environments, indicating that introducing the prior effectively reduces the multimodal ambiguity in the observation-to-state mapping.

C. KITTI Visual Odometry

Overview: We evaluate our method on the KITTI Visual Odometry dataset [11], where the objective is to track a vehicle’s pose over time using RGB images captured from a stereo camera and the given initial pose. In this task, the vehicle’s pose is not directly available from images and must be inferred by estimating relative motion across frames and accumulating it over time. This process is prone to drift, especially without loop closure. Moreover, the limited size and diversity of the dataset pose challenges for generalization to unseen road conditions.

Data: Following the protocol from [22], we adopt the KITTI-10 dataset, which comprises ten driving sequences recorded in urban environments. Each sequence includes paired stereo images and ground truth poses. The data is recorded at around 10 Hz. To expand the training data, we perform horizontal flipping on the stereo image pairs. After augmentation, sequences are segmented into fixed-length clips and downsampled to 50×150 pixels per frame.

Filter Implementation: The vehicle’s state at each time step is represented as a 5D vector $\mathbf{x}_t = (l_t^x, l_t^y, \theta_t, v_t, \omega_t)$, consistent with [22], [42]. Here, (l_t^x, l_t^y) denote the 2D position, θ_t is the heading angle, v_t is the linear velocity, and ω_t the angular rate. Observations include the current RGB frame and a difference frame computed by subtracting the previous frame, following [41] (see Fig. 6). We use 10 particles in our filter. Since explicit control inputs are not



Fig. 6: Each row shows an example from a different sequence: (Left) frame at $t-1$, (Middle) current frame, and (Right) the corresponding difference frame.

available, we adopt a constant velocity and angular velocity model as the process model, where the change in velocities between consecutive time steps is treated as process noise. The sensor model for observed images reuses the backbone architecture from [22], [42]. We encode the observation \mathbf{o}_t using the sensor model and flatten the predicted particle

set $\{\hat{\mathbf{x}}_t^{(i)}\}_{i=1}^N$ into a vector. The two are concatenated to form the conditional input \mathbf{c}_t for the diffusion model. The denoising network in diffusion model is instantiated as a same 3-layer U-Net. The training employs a 10-fold cross-validation setup, where nine trajectories are used for training and the remaining one for testing in each fold. The model is pretrained solely based on visual observations, the particle set is introduced in a subsequent training stage.

Results: We use 10 diffusion steps and evaluate on 100-frame segments following KITTI’s standard metrics. Positional and angular errors are computed by comparing the final predicted pose to the ground truth and normalizing by the total traveled distance (m/m and deg/m, respectively).

To ensure a more thorough evaluation, a diverse set of baseline models is selected for comparison:

1) Differentiable Filters: Include several state-of-the-art differentiable recursive filters proposed in previous studies [22], [35], [41]. To ensure a fair evaluation, we adopt the same input and use identical sensor model architectures.

2) LSTMs: Building on previous research in differentiable filtering [22], [41], we include long short-term memory (LSTM) models [44]. We choose an unidirectional LSTM and a LSTM integrated with dynamics as the baselines [22].

3) Smoothers: We adopt the differentiable smoothers introduced in [42], which are built upon factor graph optimization. As these methods utilize the full observation sequence, they naturally hold an advantage over filtering-based approaches.

All of the experimental results are presented in Table IV.

TABLE IV: Performance comparison of DiffPF and baseline models on KITTI dataset.

Setting	Methods	m/m	deg/m)
Ours	DiffPF	0.126 ± 0.019	0.0549 ± 0.005
Differentiable Filter	dUKF	0.180 ± 0.023	0.0799 ± 0.008
	dEKF	0.168 ± 0.012	0.0743 ± 0.007
	dPF-M-lrn	0.190 ± 0.030	0.0900 ± 0.014
	dMCKUF	0.200 ± 0.030	0.0820 ± 0.013
LSTM	LSTM (uni.)	0.757 ± 0.012	0.3779 ± 0.054
	LSTM (dy.)	0.538 ± 0.057	0.0788 ± 0.008
Smother, Heteroscedastic	E2E Loss, Vel	0.148 ± 0.009	0.0720 ± 0.006
	E2E Loss, Pos	0.146 ± 0.010	0.0762 ± 0.007

Comparison: Our DiffPF achieves a 25% reduction in position error and a 26% reduction in orientation error compared to leading differentiable filtering approaches. It also surpasses LSTMs and differentiable smoothers in performance. These results highlight the strength of the diffusion model in capturing complex posterior distributions, enabling more effective particle sampling and higher-quality approximations of the posterior. Furthermore, the method operates at 46.5 Hz, well above the 10 Hz input rate of the visual stream, ensuring its suitability for real-time applications.

V. CONCLUSIONS

In this work, we proposed **DiffPF**, a novel differentiable particle filtering framework that integrates diffusion models into the recursive Bayesian estimation pipeline. Our method replaces traditional update mechanisms—typically reliant on

hand-designed proposals and importance weighting—with a learned denoising process that enables flexible, fully differentiable, and high-quality sampling from complex posteriors. By modeling the update step with a conditional diffusion model, DiffPF is capable of capturing multimodal distributions, mitigating particle degeneracy, and eliminating the need for resampling. This design leads to more expressive and robust belief representations compared to existing differentiable particle filters. We validate the effectiveness of DiffPF across a variety of simulated and real-world tasks. Experimental results consistently show superior state estimation accuracy over strong baselines, demonstrating the generality and robustness of our approach.

Future work will focus on optimizing inference speed to better suit real-time applications and extending the framework to leverage richer sensory inputs and global correction techniques such as loop closure.

REFERENCES

- [1] S.-Y. Chen, “Kalman filter for robot vision: a survey,” *IEEE Transactions on industrial electronics*, vol. 59, no. 11, pp. 4409–4420, 2011.
- [2] E. Kaufmann, L. Bauersfeld, A. Loquercio, M. Müller, V. Koltun, and D. Scaramuzza, “Champion-level drone racing using deep reinforcement learning,” *Nature*, vol. 620, no. 7976, pp. 982–987, 2023.
- [3] L. Wang, G. Wang, S. Jia, A. Turner, and S. Ratchev, “Imitation learning for coordinated human–robot collaboration based on hidden state-space models,” *Robotics and computer-integrated manufacturing*, vol. 76, p. 102310, 2022.
- [4] S. Thrun, W. Burgard, and D. Fox, *Probabilistic Robotics (Intelligent Robotics and Autonomous Agents)*. The MIT Press, 2005.
- [5] N. J. Gordon, D. J. Salmond, and A. F. Smith, “Novel approach to nonlinear/non-gaussian bayesian state estimation,” in *IEE proceedings F (radar and signal processing)*, vol. 140, no. 2. IET, 1993, pp. 107–113.
- [6] K. Murphy and S. Russell, “ Rao-blackwellised particle filtering for dynamic bayesian networks,” in *Sequential Monte Carlo methods in practice*. Springer, 2001, pp. 499–515.
- [7] S. S. Rangapuram, M. W. Seeger, J. Gasthaus, L. Stella, Y. Wang, and T. Januschowski, “Deep state space models for time series forecasting,” *Advances in neural information processing systems*, vol. 31, 2018.
- [8] X. Chen and Y. Li, “An overview of differentiable particle filters for data-adaptive sequential bayesian inference,” *arXiv preprint arXiv:2302.09639*, 2023.
- [9] R. Jonschkowski, D. Rastogi, and O. Brock, “Differentiable particle filters: End-to-end learning with algorithmic priors,” *arXiv preprint arXiv:1805.11122*, 2018.
- [10] P. Karkus, D. Hsu, and W. S. Lee, “Particle filter networks with application to visual localization,” in *Conference on robot learning*. PMLR, 2018, pp. 169–178.
- [11] A. Geiger, P. Lenz, C. Stiller, and R. Urtasun, “Vision meets robotics: The kitti dataset,” *The International Journal of Robotics Research*, vol. 32, no. 11, pp. 1231–1237, 2013.
- [12] P. M. Djuric, J. H. Kotecha, J. Zhang, Y. Huang, T. Ghirmai, M. F. Bugallo, and J. Miguez, “Particle filtering,” *IEEE signal processing magazine*, vol. 20, no. 5, pp. 19–38, 2003.
- [13] S. Godsill, “Particle filtering: the first 25 years and beyond,” in *ICASSP 2019-2019 IEEE International Conference on Acoustics, Speech and Signal Processing (ICASSP)*. IEEE, 2019, pp. 7760–7764.
- [14] A. Doucet, S. Godsill, and C. Andrieu, “On sequential monte carlo sampling methods for bayesian filtering,” *Statistics and computing*, vol. 10, pp. 197–208, 2000.
- [15] M. K. Pitt and N. Shephard, “Filtering via simulation: Auxiliary particle filters,” *Journal of the American statistical association*, vol. 94, no. 446, pp. 590–599, 1999.
- [16] F. Septier and G. W. Peters, “Langevin and hamiltonian based sequential mcmc for efficient bayesian filtering in high-dimensional spaces,” *IEEE Journal of selected topics in signal processing*, vol. 10, no. 2, pp. 312–327, 2015.
- [17] C. Andrieu, A. Doucet, and R. Holenstein, “Particle markov chain monte carlo methods,” *Journal of the Royal Statistical Society Series B: Statistical Methodology*, vol. 72, no. 3, pp. 269–342, 2010.
- [18] X. Chen and Y. Li, “Normalizing flow-based differentiable particle filters,” *IEEE Transactions on Signal Processing*, 2024.
- [19] A. Corenflos, J. Thornton, G. Deligiannidis, and A. Doucet, “Differentiable particle filtering via entropy-regularized optimal transport,” in *International Conference on Machine Learning*. PMLR, 2021, pp. 2100–2111.
- [20] A. Šcibor and F. Wood, “Differentiable particle filtering without modifying the forward pass,” *arXiv preprint arXiv:2106.10314*, 2021.
- [21] C. Rosato, L. Devlin, V. Beraud, P. Horridge, T. B. Schön, and S. Maskell, “Efficient learning of the parameters of non-linear models using differentiable resampling in particle filters,” *IEEE Transactions on Signal Processing*, vol. 70, pp. 3676–3692, 2022.
- [22] A. Kloss, G. Martius, and J. Bohg, “How to train your differentiable filter,” *Autonomous Robots*, vol. 45, no. 4, pp. 561–578, 2021.
- [23] X. Ma, P. Karkus, D. Hsu, and W. S. Lee, “Particle filter recurrent neural networks,” in *Proceedings of the AAAI conference on artificial intelligence*, vol. 34, no. 04, 2020, pp. 5101–5108.
- [24] T. Le, M. Igl, T. Rainforth, T. Jin, and F. Wood, “Auto-encoding sequential monte carlo,” in *International Conference on Learning Representations (ICLR)*. OpenReview, 2018.
- [25] C. Naeseth, S. Linderman, R. Ranganath, and D. Blei, “Variational sequential monte carlo,” in *International conference on artificial intelligence and statistics*. PMLR, 2018, pp. 968–977.
- [26] P. Bickel, B. Li, and T. Bengtsson, “Sharp failure rates for the bootstrap particle filter in high dimensions,” in *Pushing the limits of contemporary statistics: Contributions in honor of Jayanta K. Ghosh*. Institute of Mathematical Statistics, 2008, vol. 3, pp. 318–330.
- [27] M. Zhu, K. Murphy, and R. Jonschkowski, “Towards differentiable resampling,” *arXiv preprint arXiv:2004.11938*, 2020.
- [28] J. Sohl-Dickstein, E. Weiss, N. Maheswaranathan, and S. Ganguli, “Deep unsupervised learning using nonequilibrium thermodynamics,” in *International conference on machine learning*. PMLR, 2015, pp. 2256–2265.
- [29] J. Ho, A. Jain, and P. Abbeel, “Denoising diffusion probabilistic models,” *Advances in neural information processing systems*, vol. 33, pp. 6840–6851, 2020.
- [30] C. Chi, Z. Xu, S. Feng, E. Cousineau, Y. Du, B. Burchfiel, R. Tedrake, and S. Song, “Diffusion policy: Visuomotor policy learning via action diffusion,” *The International Journal of Robotics Research*, p. 02783649241273668, 2023.
- [31] A. Sridhar, D. Shah, C. Glossop, and S. Levine, “Nomad: Goal masked diffusion policies for navigation and exploration,” in *2024 IEEE International Conference on Robotics and Automation (ICRA)*. IEEE, 2024, pp. 63–70.
- [32] Z. Wang, J. J. Hunt, and M. Zhou, “Diffusion policies as an expressive policy class for offline reinforcement learning,” *arXiv preprint arXiv:2208.06193*, 2022.
- [33] J. Carvalho, A. T. Le, M. Baierl, D. Koert, and J. Peters, “Motion planning diffusion: Learning and planning of robot motions with diffusion models,” in *2023 IEEE/RSJ International Conference on Intelligent Robots and Systems (IROS)*. IEEE, 2023, pp. 1916–1923.
- [34] Z. Liang, Y. Mu, M. Ding, F. Ni, M. Tomizuka, and P. Luo, “Adapt-diffuser: Diffusion models as adaptive self-evolving planners,” *arXiv preprint arXiv:2302.01877*, 2023.
- [35] Z. Wan and L. Zhao, “Dnd filter: Differentiable state estimation for dynamic systems using diffusion models,” *arXiv preprint arXiv:2503.01274*, 2025.
- [36] S. Särkkä and L. Svensson, *Bayesian filtering and smoothing*. Cambridge university press, 2023, vol. 17.
- [37] L. V. Jospin, H. Laga, F. Boussaid, W. Buntine, and M. Bennamoun, “Hands-on bayesian neural networks—a tutorial for deep learning users,” *IEEE Computational Intelligence Magazine*, vol. 17, no. 2, pp. 29–48, 2022.
- [38] G. Papamakarios, E. Nalisnick, D. J. Rezende, S. Mohamed, and B. Lakshminarayanan, “Normalizing flows for probabilistic modeling and inference,” *Journal of Machine Learning Research*, vol. 22, no. 57, pp. 1–64, 2021.
- [39] J. Song, C. Meng, and S. Ermon, “Denoising diffusion implicit models,” *arXiv preprint arXiv:2010.02502*, 2020.
- [40] S. Chan *et al.*, “Tutorial on diffusion models for imaging and vision,” *Foundations and Trends® in Computer Graphics and Vision*, vol. 16, no. 4, pp. 322–471, 2024.

- [41] T. Haarnoja, A. Ajay, S. Levine, and P. Abbeel, "Backprop kf: Learning discriminative deterministic state estimators," *Advances in neural information processing systems*, vol. 29, 2016.
- [42] B. Yi, M. A. Lee, A. Kloss, R. Martín-Martín, and J. Bohg, "Differentiable factor graph optimization for learning smoothers," in *2021 IEEE/RSJ International Conference on Intelligent Robots and Systems (IROS)*. IEEE, 2021, pp. 1339–1345.
- [43] C. Beattie, J. Z. Leibo, D. Teplyaev, T. Ward, M. Wainwright, H. Küttler, A. Lefrancq, S. Green, V. Valdés, A. Sadik *et al.*, "Deepmind lab," *arXiv preprint arXiv:1612.03801*, 2016.
- [44] A. Graves and A. Graves, "Long short-term memory," *Supervised sequence labelling with recurrent neural networks*, pp. 37–45, 2012.